



# OPEN Lacustrine sedimentation patterns at the Northern Antarctic Peninsula and surroundings as a response to late Holocene and Modern Climate changes

Heitor Evangelista<sup>1✉</sup>, Sergei Verkulich<sup>2</sup>, Bulat Mavlyudov<sup>3</sup>, Mariza P. Souza Echer<sup>4</sup>, Marcus Vinicius Licinio<sup>5</sup>, Gerd Dercon<sup>6</sup>, Felipe García-Rodríguez<sup>7,8</sup>, Arthur A. Neto<sup>9</sup>, Stephanie Kusch<sup>10</sup>, Rodrigo C. Abuchacra<sup>11</sup>, Anna B.J. Oaquin<sup>1</sup>, Sérgio J. Gonçalves Jr.<sup>1</sup>, Zinaida Pushina<sup>12</sup>, Marília H Shimizu<sup>13</sup>, Maria Heiling<sup>6</sup>, Johanna Slaets<sup>6</sup>, Christian Resch<sup>6</sup>, Alejandra Castillo<sup>14</sup> & Roman Gruber<sup>6</sup>

The Northern Antarctic Peninsula (NAP) and the West Antarctic Ice Sheet (WAIS) are likely to respond rapidly to climate changes by increasing the collapse of peripheral ice shelves and the number of days above 0 °C. These facts make this region a representative hotspot of the global sea level rise and the location of one of the global climate tipping points (thresholds in the Earth system whose changes may become irreversible, if exceeded). Understanding the climate evolution of the NAP, based on past evidences, may help infer its future scenario. Herein, from a comprehensive survey of lacustrine sedimentation in proglacial and periglacial lakes/ponds, we investigated the impact of climate changes on the terrestrial environment in two complementary time scales (Late Holocene and contemporary age). For the longer time scale, regional climate database and biogeochemical properties of Lake Long/NAP sediment core, suggest warming between 4.0 and 2.0 kyr BP following a cooling phase towards the present, that endorse previously suggested Late Holocene Neoglacial (LHN). We attribute the LHN phase to a combined action of long-term decline in total solar irradiance, the Andean volcanism and the El Niño Southern Oscillation. For the contemporary age, we found a rapid coupled response of atmosphere/cryosphere/lithosphere to present warming levels.

The Northern Antarctic Peninsula (NAP) and the West Antarctic Ice Sheet (WAIS) are among the regions of the most rapidly warming of the planet<sup>1</sup> since the mid-20th century, playing a pivotal role in global sea level rise<sup>2,3</sup>. WAIS has been steadily witnessing unprecedented surface snow melting events<sup>4</sup> and increasing ice sheet destabilization<sup>5</sup>. In recent decades, ground-based meteorological stations at NAP, and the surrounding region, have documented great variability in mean annual air temperature trends, including a steep warming

<sup>1</sup>LARAMG/IBRAG, Pav. Haroldo L. da Cunha. Rio de Janeiro State University, Rio de Janeiro, Brazil. <sup>2</sup>Herzen State Pedagogical University of Russia, Moyka Emb, Saint-Petersburg 191186, Russian Federation. <sup>3</sup>Russian Academy of Sciences/Institute of Geography, Staromonetny pereulok, 29, Moscow 119017, Russian Federation. <sup>4</sup>INPE (National Institute of Space Research), Av. Dos Astronautas s/n. São José dos Campos, Cuiaba, SP, Brazil. <sup>5</sup>Departamento de Ciências Fisiológicas, Centro de Ciências da Saúde CCS – UFES. Maruipé, Vitória, ES, Brazil. <sup>6</sup>Soil and Water Management & Crop Nutrition Laboratory, Joint FAO/IAEA Centre of Nuclear Techniques in Food and Agriculture, International Atomic Energy Agency, Vienna, Austria. <sup>7</sup>Universidad de la República, Centro Universitario Regional Este, CURE, Rocha, Uruguay. <sup>8</sup>Instituto de Oceanografía, Programa de Pós-Graduação em Oceanologia, Universidade Federal de Rio Grande, Rio Grande, Brazil. <sup>9</sup>Laboratório de Geologia Marinha/LAGEMAR, Universidade Federal Fluminense, Niterói, Brazil. <sup>10</sup>Institut des Sciences de la Mer (ISMER), Université du Québec à Rimouski, Rimouski, Canada. <sup>11</sup>Department of Geography, Graduate Program in Geography, State University of Rio de Janeiro (UERJ-FFP), Rua Dr. Francisco Portela, São Gonçalo 1470, 24435-005, RJ, Brazil. <sup>12</sup>Arctic and Antarctic Research Institute, St. Petersburg, Russian Federation. <sup>13</sup>General Coordination of Earth Science (CGCT), National Institute for Space Research (INPE), São José dos Campos, Brazil. <sup>14</sup>Instituto de Ciencias Químicas, Facultad de Ciencias, Universidad Austral de Chile, Las Encinas 220, Valdivia, Chile. ✉email: evangelista.uerj@gmail.com

of  $0.32 \pm 0.20$  °C between 1979 and 1997 and a relative cooling period of  $-0.47 \pm 0.25$  °C between 1999 and 2014<sup>6</sup>. In February 2020, Esperanza Base located at the NAP/Graham Land (Lat. 63 °S) recorded a maximum annual air temperature of +18.3 °C (SMN-Servicio Meteorológico Nacional from Argentina - <https://www.smn.gob.ar/>), officially the warmest temperature ever instrumentally recorded in Antarctica as announced by the World Meteorological Organization (WMO). These short-term successive temperature increases and reversals illustrate how unpredictable the climate at the NAP has become in recent decades.

Part of the complexity in describing the climate of the NAP is due to its location in a climatic transition zone influenced by the temperate North, when air masses derive from the South Pacific or Southern South America, and the polar South, when coming from the Weddell Sea or Bellingshausen Sea<sup>7</sup>. Several controls (or combined effects of them) have been proposed to explain the climate variability at NAP (and WAIS), which includes atmosphere-ocean coupling linked to the Tropical Pacific<sup>8</sup>, El Niño Southern Ocean (ENSO)<sup>9</sup>, anthropogenic amplification of the circumpolar westerlies via greenhouse gases (GHG) and ozone depletion<sup>10</sup>, the Southern Hemisphere Annular Mode (SAM)<sup>11</sup>, phase coupled ENSO-SAM<sup>12</sup>, the action of atmospheric rivers<sup>13</sup> and intrusions of Warm Circumpolar Deep Water<sup>14</sup>. For longer time scales, retrieving the Holocene climate history of the NAP based on proxy records, has been a challenging issue.

Attempts to recover air temperature records from ice cores based on isotope analysis were rarely successful at the NAP because of intense summer melting detected at locations below 1,000 m. At these altitudes, the glacial-chemical record is modified due to vertical ionic elution along the core profiles<sup>15</sup> and the seasonal and interannual variability of oxygen and hydrogen isotopes are not well preserved due to water percolation and refreezing and therefore they do not allow the regional climatic history. Few works (e.g.: Fernandoy *et al.*, 2012<sup>16</sup>) were successful at altitudes above 1,000 m although they could not retrieve more than a decade of climatic history. In contrast, analysis of near-shore glaciomarine sediment deposits may reveal consistent interplay among the glaciogenic, oceanographic, climatic, and physiographic compartments<sup>17</sup>. However, at shallow sites, ice scouring from icebergs or other floating ice masses may gouge the seafloor and disturb the surface sediment distribution.

In the context of the NAP (extensible to all Maritime Antarctica), the lacustrine environment emerges as an alternative to provide insights into past climate changes that can extend back far beyond the instrumental epoch. As depositional systems, they receive fluxes of mineral dust and chemical compounds from the atmospheric fallout. Throughout the Holocene, these sites witnessed the transition from an underneath glacier environment into an ice-free region becoming genuine proglacial lakes. As a result, the bottom lake sediments preserve physical properties and biogeochemical compounds from which we can assess past productivity, temperature, runoff, and atmospheric circulation.

In this work, we investigate the past climate changes at NAP, and the surrounding region, from two sedimentary records dated for different (complementary) time scales: (1) modern sedimentation enclosing approximately the last 120 years retrieved from 8 (eight) lakes/ponds in the proglacial environment<sup>18</sup> of King George Island (KGI)/South Shetland Islands (these lakes are located close to the ice front of glaciers, Fig. 1d); and (2) from 15 (fifteen) Holocene periglacial/isolated lakes (located away from the glacier front) Fig. 1a, c. Combining these two databases, we can better recover the sedimentary history (and associated climate/environmental history) for the study region. This approach may also allow the comparison of sedimentary records with ice core and deep ice borehole data, as well as determine the role of natural climate forcing (total solar irradiance, insolation, ENSO, volcanism and CO<sub>2</sub>).

## Site description

### King George Island (KGI) climate, proglacial/periglacial environment

King George Island (KGI) is the largest island of the South Shetland archipelago, located at the northwestern end of the NAP, between 61°54'S-62°06'S and 057°35'W-059°02'W. Most of the air masses acting at KGI derive from the Pacific sector of the Southern Ocean (classified as maritime polar; mP), from advection north and northwest of 60°S latitude (classified as maritime tropical; mT)<sup>19</sup>, and cold air incursions from continental Antarctica that bring extremely low temperatures to the region. The western NAP is warmer and more humid and is characterized by a smaller sea ice seasonal extent, whereas the eastern sector is colder and more susceptible to Antarctic inland air flow with lower air temperatures and humidity<sup>6</sup>.

Albeit infrequent, liquid precipitation has been reported at almost all stations in the South Shetland Islands. Liquid precipitation, besides air temperature, has been considered a factor that directly impacts regional mass balance through modulation of the surface albedo and the acceleration of glaciers' retreat by eroding the ice or through hydrofracturing when associated with surface melting. At King George Island, Bellingshausen station has reported an average summer precipitation of 165 mm yr<sup>-1</sup> between 1969 and 2017 (this issue).

Proglacial lakes investigated are located at Admiralty Bay/KGI ice-free areas (Fig. 1b) while periglacial lakes at Fildes Peninsula/KGI and the surrounding region, Fig. 1. Admiralty Bay is formed by irregular fjords of tectonic origin containing inlets and coves and a deep main channel reaching a maximum depth of 535 m. Fildes Peninsula is the largest ice-free area in extent and is located in the Southwestern sector of KGI bordered by the Drake Passage, the Maxwell Bay and the Bellingshausen ice dome. Due to depressions created during moraine formation and the action of fluvial drainage networks in ice-free areas from melting freshwater discharge during deglaciation, a lake sequence is found across the peninsula. This process was relatively common in most domains of the South Shetland Islands<sup>20</sup>.

## Results

### Modern sedimentation: an atmosphere-cryosphere-lithosphere coupled system

The composite of the air temperature curve used in this work is derived from 3 meteorological stations at South Shetland Islands (Bellingshausen, March and Deception) (Mean annual data is presented in Supplementary

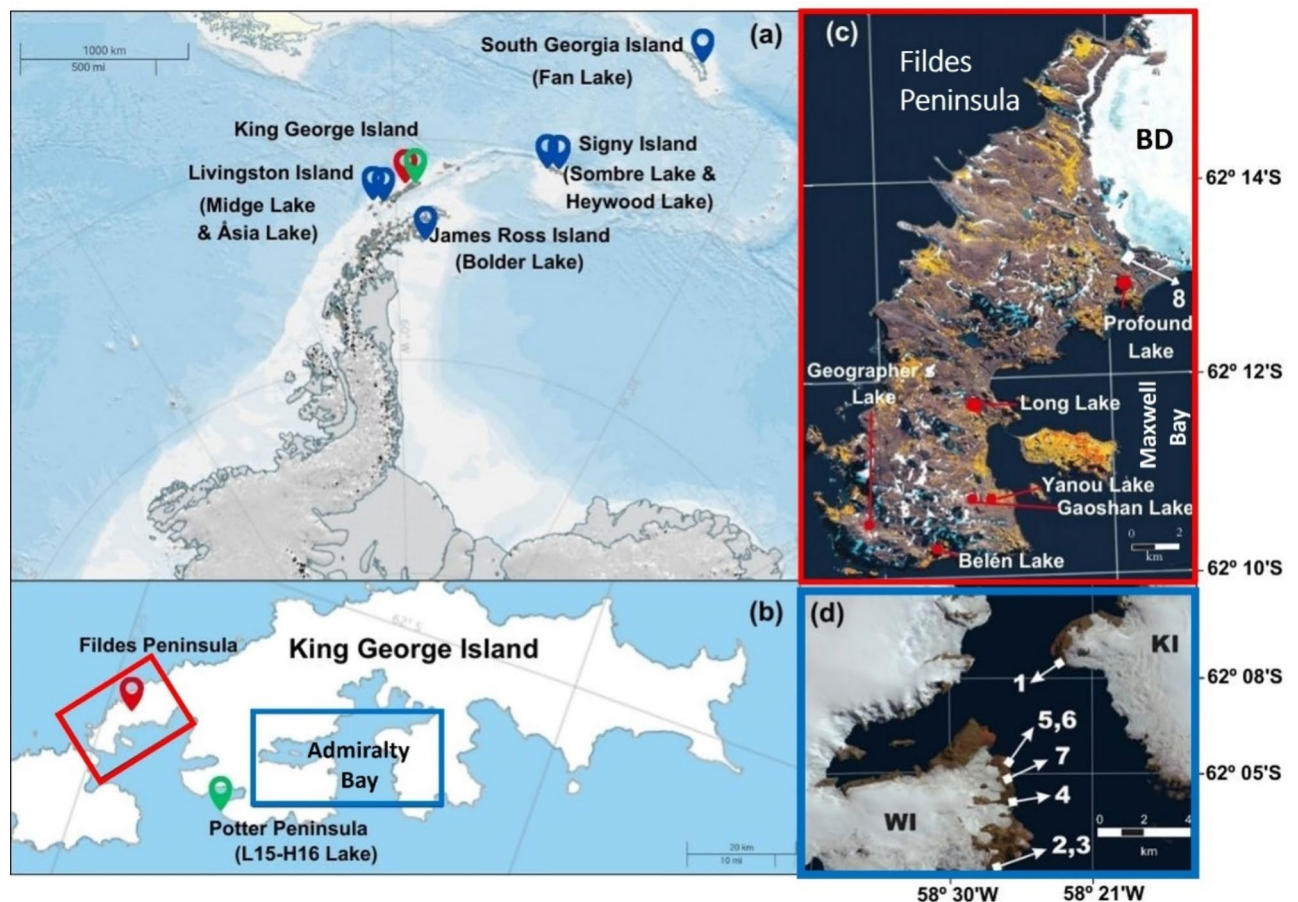


**Fig. 1.** Sediment Coring Locations. (a) Surveyed isolated lakes at the North Antarctic Peninsula, NAP, and the surrounding region (blue dots). Lakes at King George Island, KGI, are denoted by a red dot (this issue) and a green dot; (b) KGI and 2 boxes indicating the location of the two largest ice-free areas (Fildes Peninsula and Admiralty Bay) and Potter Peninsula; (c) Detail of Fildes Peninsula with locations of isolated lakes investigated in this study (red squares). Exception for point 8 (proglacial lake); (d) Detail of Admiralty Bay with locations of periglacial lakes/ponds (white squares from 1 to 7); BD: Bellingshausen Dome, WI: Warszawa Icefield and KI: Krakow Icefield. Source: (a) (b) (c) - adapted from the Natural Environment Research Council (NERC)-BAS (<http://www.antarctica.ac.uk>) after editions at Roberts et al. (2017); (d) - modified from the original SPOT satellite image 23fev2000 from the archives of the Brazilian Antarctic Program, PROANTAR/CNPq.

information 2). The mean annual air temperature curve shows that from the 1970s to the first decade of the 21st century, regional levels increased by 2 °C with a peak around the year 2000 following a drop of 1 °C in the subsequent years, Fig. 2. Following this pattern, Equilibrium Line Altitude (ELA)<sup>21</sup> (the altitude where accumulation equals ablation over a 1-year period) presented a similar behavior, i.e., changing more than 100 m in the same period at Bellingshausen Dome/KGI. The method for ELA estimation at KGI is fully described at Mavlyudov, 2023<sup>21</sup>. It should be noted that the sequential climatic response presented in Fig. 2 was inferred from Maritime Antarctic glaciers, which are notably more sensitive to changes in air temperatures as demonstrated in previous studies<sup>22</sup> and cannot be generalized to drier continental-type glaciers.

The time scale of these observations comprises an interval compatible with the dating of modern sedimentation processes at lakes/ponds close to glacier fronts in rapid retraction processes. They receive melting water during the summer season or during rapid warming episodes along the year. <sup>210</sup>Pb excess technique allow an age-depth estimation for sediment core profiles of these periglacial shallow lakes. From the Constant Rate of Supply (CRS) model (see methods) applied to the <sup>210</sup>Pb excess activities measured at each stratification of the sediment cores, we obtained the sedimentation rates from eight lakes at proglacial sites in KGI (Supplementary information 3). In this case, Ti/Ca and Ti/Al ratios, obtained by XRF at Lake Profound sediment core<sup>23</sup>, widely known to be very sensitive to changes in terrigenous input (e.g.: Mesa-Fernández et al., 2022<sup>24</sup>) can be here interpreted as proxies for catchment erosion/runoff, since their variability corresponded to peaks at the sedimentation curve, as shown in Fig. 2.



## Sequential climatic response for the Maritime Antarctic environment

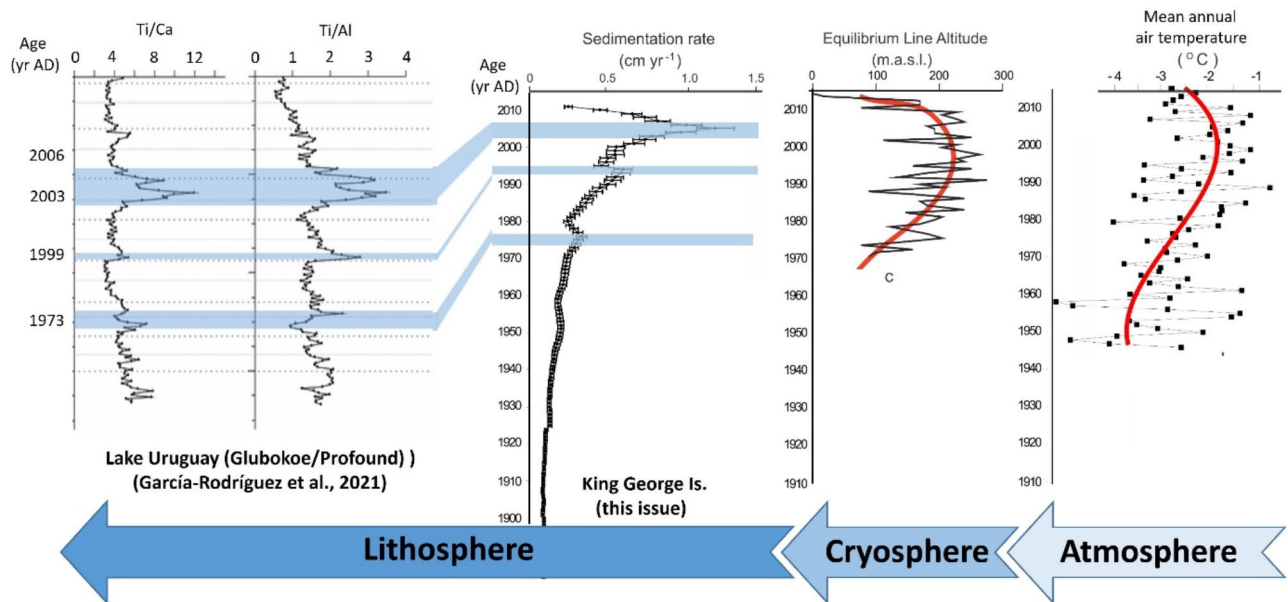


**Fig. 2.** Atmosphere-Cryosphere-Proglacial environment climatic responses. Sequential climatic response at North Antarctic Peninsula (from right to left): instrumental mean annual air temperature (South Shetland Islands air temperature composite is formed by data from the stations: Bellingshausen, March, Comandante Ferraz and Deception - Supplementary information 2), Equilibrium Line Altitude for Bellingshausen Dome (Mavlyudov, 2023), mean lacustrine sedimentation for eight proglacial lakes (Fig. 1), (this issue), and Lake Profound XRF data (García-Rodríguez et al., 2021) as a proxy for catchment erosion/runoff. Sedimentation rate time series was obtained from the chronological model CRS that provided the age of each sediment depositional layer and then arranged vertically. Three events of sedimentation rate peaks observed in this work (light blue rectangles) corresponded to changes in Ti/Ca and Ti/Al ratios from sediment layers presented in García-Rodríguez et al. (2021) work for Lake Profound at Fildes Peninsula. The time scale for Ti/Ca and Ti/Al series is enlarged to fit the upper layers sedimentation peaks.

### Late Holocene sedimentation

For the Late Holocene period, the sedimentary history was inferred from the sediment core-top ages enclosing 15 surveyed lakes in NAP and the surrounding region (ice-free areas at Fildes Peninsula/KGI, Potter Peninsula/KGI, James Ross Island, Signy Island, South Georgia Island, and Livingston Island) (Table 1). In this work, we added 4 new core surface datings to the regional database for Holocene periglacial (isolated) lakes at Fildes Peninsula: Lakes Profound, Long (Supplementar information 3), Slamnoe (AMS ID D-MAS 051940), Trigrorskoe (AMS ID D-AMS 051938) and Geographensee (AMS ID D-MAS 051934). All ages presented in Table 1 were performed by radiocarbon, expressed as  $^{14}\text{C}$  cal yr BP, and are related to top-surface sediment sections of the cores (mostly within the top 5 cm as presented in the literature or performed in the present work). The ancient dates found for sediment core – tops of the surveyed Holocene periglacial (isolated) lakes mean that they have not experienced sedimentation since that time. We interpret this finding as representing a regional cooling climate phase when no significant sedimentation took place after so. Geological surveys at King George Island indicate that limestone occurrences are basically formed by erratic fossiliferous boulders<sup>25</sup>, and therefore might not represent significant sources of “old carbon” to the bottom surface sediments. Additionally, some references employed small fragments of plants to date the core-top sediment sections (as mosses) in a stand of bulk sediments.

The variability in core-top ages in Table 1 may reflect the action of different processes as sampling, lake geomorphology, lake depth, the amount of fine sediments existing around the lakes (available to runoff), the amount of winter snow accumulated in its borders and possibly other factors. Besides that, different age-depth models were applied to the database by the original authors. Finally, the survey was taken in a regional context, from a northern limit on South Georgia Island (latitude 54°–55°S) to a southern limit on James Ross Island (latitude 64°S), from the Western and Eastern sides of the Antarctic Peninsula, influenced by the Bellingshausen Sea and Weddell Sea, respectively, and further north where the marine influence is very high.

Lake name	Location	Core-top age	References
		<sup>14</sup> C cal. yr BP	
Bolder	James Ross Island	≈ 1530	Bjorck et al., 1996 <sup>26</sup>
Yanou	Fildes Peninsula, King George Island	≈ 768	Watcham et al., 2011 <sup>2</sup>
Belén	Fildes Peninsula, King George Island	≈ 382	Watcham et al., 2011 <sup>2</sup>
Gaoshan	Fildes Peninsula, King George Island	≈ 1087	Watcham et al., 2011 <sup>2</sup>
L15-H16	Potter Peninsula, King George Island	≈ 540	Barión et al., 2023 <sup>27</sup>
Midge	Livingston Island	≈ 605	Bjorck et al., 1991 <sup>28</sup>
Asa	Bayers Peninsula, Livingston Island	≈ 450	Bjorck et al., 1993 <sup>29</sup>
Sombre	Signy Island	≈ 1420	Jones et al., 2000 <sup>30</sup>
Heywood	Signy Island	≈ 340	Jones et al., 2000 <sup>30</sup>
Fan	South Georgia Island	≈ 781	Strother et al., 2015 <sup>31</sup>
Profound	Fildes Peninsula, King George Island	≈ 1074	Piccini et al., 2024 <sup>32</sup>
Long	Fildes Peninsula, King George Island	≈ 1700	this issue, 2024
Slamnoe	Fildes Peninsula, King George Island	≈ 3883	this issue, 2024
Trigorskoe	Fildes Peninsula, King George Island	≈ 758	this issue, 2024
Geographensee	Fildes Peninsula, King George Island	≈ 600	this issue, 2024

**Table 1.** Literature survey of ages of sediment core – tops from North Antarctic Peninsula and surround region.

Late holocene climate imprint in sediment core

Long Lake exhibited laminated sedimentary features (from the X-ray image) with roughly even-spaced light and dark density band formation. This structure reveals sequential deposition of organic clay-rich material (dark-colored) interbedded with silty to sandy material (light-colored). The low-energy hypoxic to anoxic bottom water conditions and the low inner circulation strength, typical of Sub-Antarctic lakes, may promote the laminated sedimentary profile and its preservation. The formation of these laminated structures commonly found in temperate, subpolar, and proglacial environments represents successive cold-to-warm climatic phases. Relationships between laminated sediment layers and climatic variability are well documented in the literature through several locations<sup>33</sup> mostly indicating annual resolution. The light-colored deposits correspond to the melting (warmer) periods, and the dark-colored laminae correspond to colder periods, as supported by the covariability detected in the upper part of the record for the C(%) and N(%) data. TEX<sub>86</sub> data (recovered only from the top 23 cm) indicated colder temperatures in this phase, probably due to cold waters entering the lake via runoff of melting water. For KGI, sequential light-and-dark sedimentary bands point to vigorous centennial-scale climate processes taking place at NAP during the Late Holocene which could be more significant than the annual climate swing.

The laminated pattern is observed throughout the core and is more evident within the upper 50 cm depth. The physical and biogeochemical properties of the sediment core indicate both marine and terrestrial lacustrine sedimentation histories. The detection of salt-intolerant diatoms in the uppermost units of the core (top 50 cm), Fig. 3a, as the species *Achnanthisdium australexiguum*, suggests a terrestrial phase of the lake, as previously described for islands located at the NAP and the surrounding region<sup>34</sup>. This is corroborated by the abrupt change in total C and N in the sediment core. They were enhanced substantially when the terrestrial phase (approximately 4.2 cal kyr BP) was established. Long Lake is located approximately 300 m from the shoreline at an elevation of only 14 m a.s.l. Its first isolation is estimated to have occurred at 6.445 ± 40 <sup>14</sup>C yr BP(7.360 cal yr BP)<sup>35</sup>. From the base of the core, dated from 6.764 cal yr BP, to approximately 4.0 cal kyr BP the X-ray radiograph depicts a pattern of less intense sedimentary oscillations compared to the above sections until the core-top. This marks a transition from marine to terrestrial environment at Lake Long site during the mid-Holocene isostatic uplift of the South Shetland Islands, due to deglaciation and tectonics<sup>35</sup>. Nearly 4.0 kyr cal BP the lake is definitively isolated what is supported by the geochemical analysis and the abundance of the diatom species *Achnanthisdium australexiguum*. Looking in a detailed sedimentary section (5–10 cm from top to bottom) of the dark-and-light sequence (grey scale/density profile), TEX<sub>86</sub> (a temperature proxy related to the cyclization of isoprenoidal GDGT (glycerol dialkyl glycerol tetraether) lipids produced by archaea), light layers correspond to colder phases. TEX<sub>86</sub> correlates positively and linearly with sea surface and freshwaters temperature<sup>36</sup>. TEX<sub>86</sub> reduction in light-colored deposits, Fig. 3b, may indicate an inflow of colder meltwaters into the lake. Darker layers correspond to more biologically productive periods when total C and N increase in the lake. However, around the top-12 cm, which corresponds to 2.3 kyr BP (according to our age-depth model in Supplementary information 4), C and N started to decline nearly coincident with the onset of the neo-glacial phase of NAP and the surrounding region.

Discussion

For the modern period, peaks of sedimentation rate at KGI occurred around 1973, 1999, and 2003/2004 corresponding to increases in terrigenous Ti/Ca and Ti/Al ratios detected in Profound Lake (Glubokoe) sediment core retrieved in the vicinity of the Bellingshausen dome<sup>23</sup> (Fig. 2). This suggests a high sensitivity of the

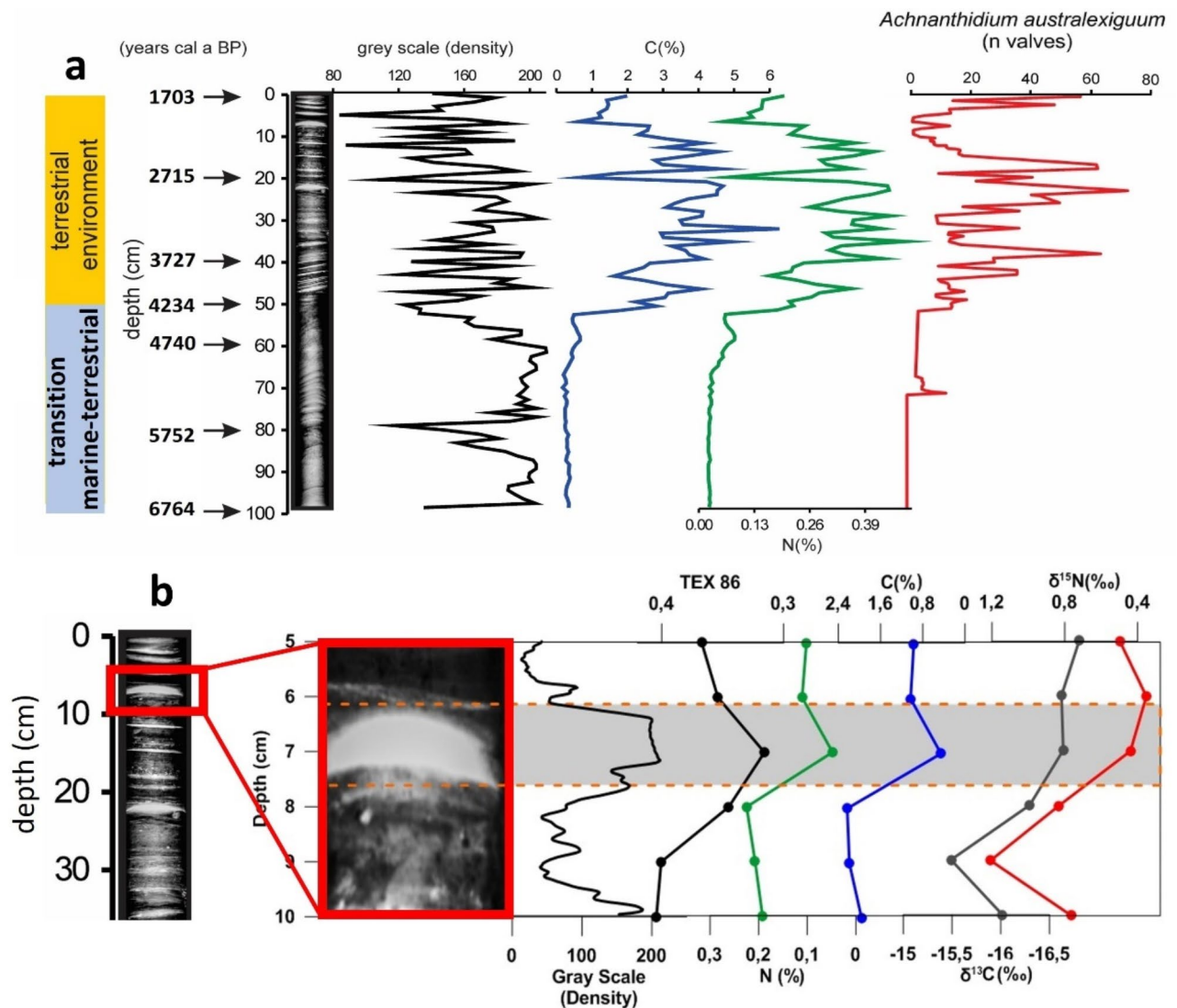


**Fig. 3.** Biogeochemistry of Long Lake core. (a) X-ray radiograph of the Long Lake core/KGI accompanied by the grayscale/density profile and biogeochemical profiles of C (%), N (%) and diatom species *Achnanthisdium australexiguum*; (b) detail of section. (5–10 cm from top to bottom) of dark-and-light stratification with additional data of TEX<sub>86</sub>,  $\delta^{13}\text{C}$  and  $\delta^{15}\text{N}$ .

proglacial/glacial system to warming events recorded in ground stations. Therefore, the lacustrine sedimentation rates and the elemental ratios of Ti/Ca and Ti/Al can be used as potential proxies for climate variability and meltwater discharge at the NAP. In the terrestrial environment of Maritime Antarctica, Ti sources are associated to sediments in the catchments, volcanism and from local wall rock erosion (the aeolian component can be only greatly enhanced during the glacial period). Ti is related to siliciclastic input of lithological origin and Ca reflects authigenic carbonate content, therefore Ti/Ca ratio can be used as a proxy for the influx of terrestrial material<sup>37</sup>.

In the geographical context, the NAP and the surrounding region are subjected to different synoptic climatic regimes (i.e. a western sector strongly influenced by air mass advection from the Pacific subtropical ocean and the westerly winds, and an eastern sector influenced by the Weddell Gyre, Southern Atlantic Ocean and polar advection). Despite these differences, a comparison between the 20th century modeled glacier surface snow melting, calculated for KGI (see Supplementary information 3), and the annual (July–June) melt percentage at JRI (melting events)<sup>4</sup> showed good agreement (Fig. 4a), thus evidencing the regional impact of modern warming at that site. The geomorphological feature of the Antarctic Peninsula constrains the westerly winds in a way that air masses while crossing the Peninsula relieve warm adiabatically as they descend towards the eastern Antarctic Peninsula<sup>38,39</sup> where JRI is located (Fig. 4b). This process also weakens the colder easterly wind, due to a stronger westerly wind acting in NAP since the 70's decade<sup>40</sup>.

Considering the fact that liquid precipitation can strongly enhance glaciers' ice mass loss by eroding the ice surface at the ablation zone and through hydrofracturing during intense surface melting<sup>41</sup>, we have also considered this parameter as a potential driver in the sedimentation issue. Melting water may carry sediments

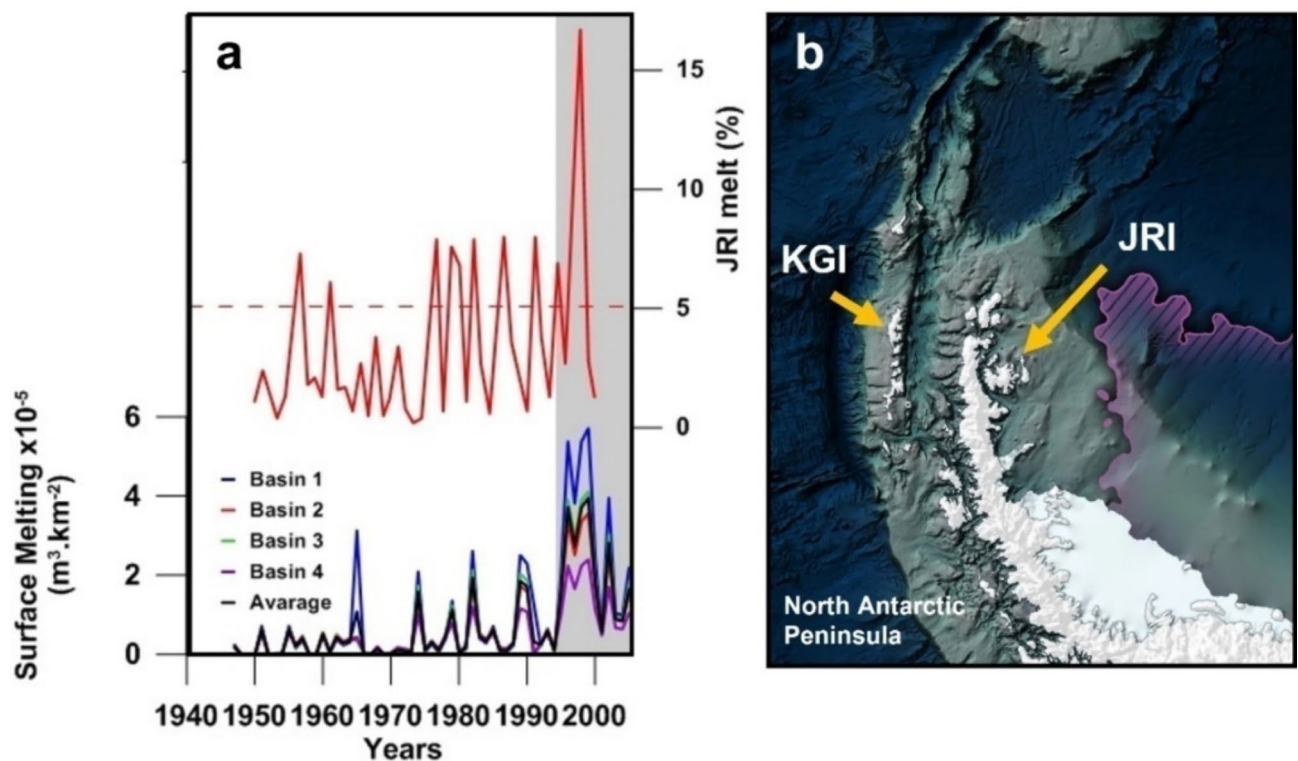


**Fig. 4.** Melting events around the North Antarctic Peninsula. **(a)** Annual (July–June) melt percentage at JRI (James Ross Island), East Antarctic Peninsula, Abram et al. (2013)<sup>4</sup>, and modeled surface melting at KGI (this issue), West Antarctic Peninsula, at 4 drainage basins (details in Supplementary information 1). The shaded box highlights the melting peak event; **(b)** location of KGI (west side) and JRI (east side).

eroded from the glacier bed, sediment-filled surface depressions and the local terrain ahead of the glaciers front into proglacial lakes (an example is illustrated in Fig. 5f in Admiralty Bay). In Fig. 5 we compared the proglacial sedimentation since 1946 at KGI (Fig. 5a) with the regional summer temperature, DJF, (composite of data from Bellingshausen–March–Condandante Ferraz–Deception stations), Fig. 5b, with the annual number of days with rain and rain + drizzle<sup>42</sup> from Rothera and Faraday–Vernadsky Stations, Fig. 5d, and summer precipitation from Bellingshausen Station at Fildes Peninsula, Fig. 5e.

The Summer Southern Annular Mode (SAM) Fig. 5c, was also included in the analysis since it is the leading mode of extratropical Southern Hemisphere climate variability, associated with the positioning and strength of the polar jet that modulates the inflow of heat and moisture to high latitudes<sup>43</sup>. None of the observed precipitation data could explain the mean proglacial sedimentation pattern presented in Fig. 5a. Precipitation showed slight increases during the 90's decade, contrasting with the peak of sedimentation rates that occurred from the mid-90s to the first decade of the 21st century, Fig. 5b/d/e.

From Fig. 5g, air temperature and sedimentation rate are significantly correlated ( $p < 0.05$ ) with lag of 0–10 years. Despite the several parameters that may define the ice mass loss, air temperature play a major role in the dynamics of the ELA, glacier mass balance and consequently the sedimentation at the proglacial environment. Previous works conducted at the Ecology Glacier/King George Island concluded that an increase in mean annual air temperature of 1 °C may enhances glacier ablation as high as 15%<sup>44</sup>. The temporal lag observed between the two parameters (warming and sedimentation) can be attributed to uncertainties of the dating method for the sedimentation the use of several proglacial lake data to calculate the mean sedimentation rate (Fig. 2) and hydrofracturing of the glacial body that allow the surface melting water to percolate, refreeze in subglacial cavities and then discharge the freshwater into proglacial channels. Our observations are in accordance with conclusions of Zhang et al. (2023)<sup>45</sup> from a broad investigation of erosion and sediment transport in cold regions in which peak sediment yield is reached with or after peak meltwater. Concurrently, the impact of SAM on the change in sedimentation rate is evident, since its positive phase is related to warmer conditions at NAP.

For the longer time scale considering the Late Holocene, our survey of isolated lakes at periglacial environments shows that they have experienced successive sedimentation hiatuses in time, as air temperature became progressively lower, characterizing a Neoglacial phase. This result is consistent with the last 2.0 kyr air temperature inferred from mean borehole temperature (black thick line in Fig. 6) at WAIS (West Antarctic Ice Sheet) Divide (79°28'S, 112°05'W, 1766 m a.s.l.), to be on average  $0.52 \pm 0.28^\circ\text{C}$  colder than the last 100-year average<sup>46</sup>. Gathering the glaciological data and the fact that 64% of the surveyed periglacial lakes have experienced sedimentation hiatuses between 200 and 800 year BP and 100% up to 340 year BP, it is consistent with the premise that the Little Ice Age (LIA) period did take place at a large portion of western Antarctica and



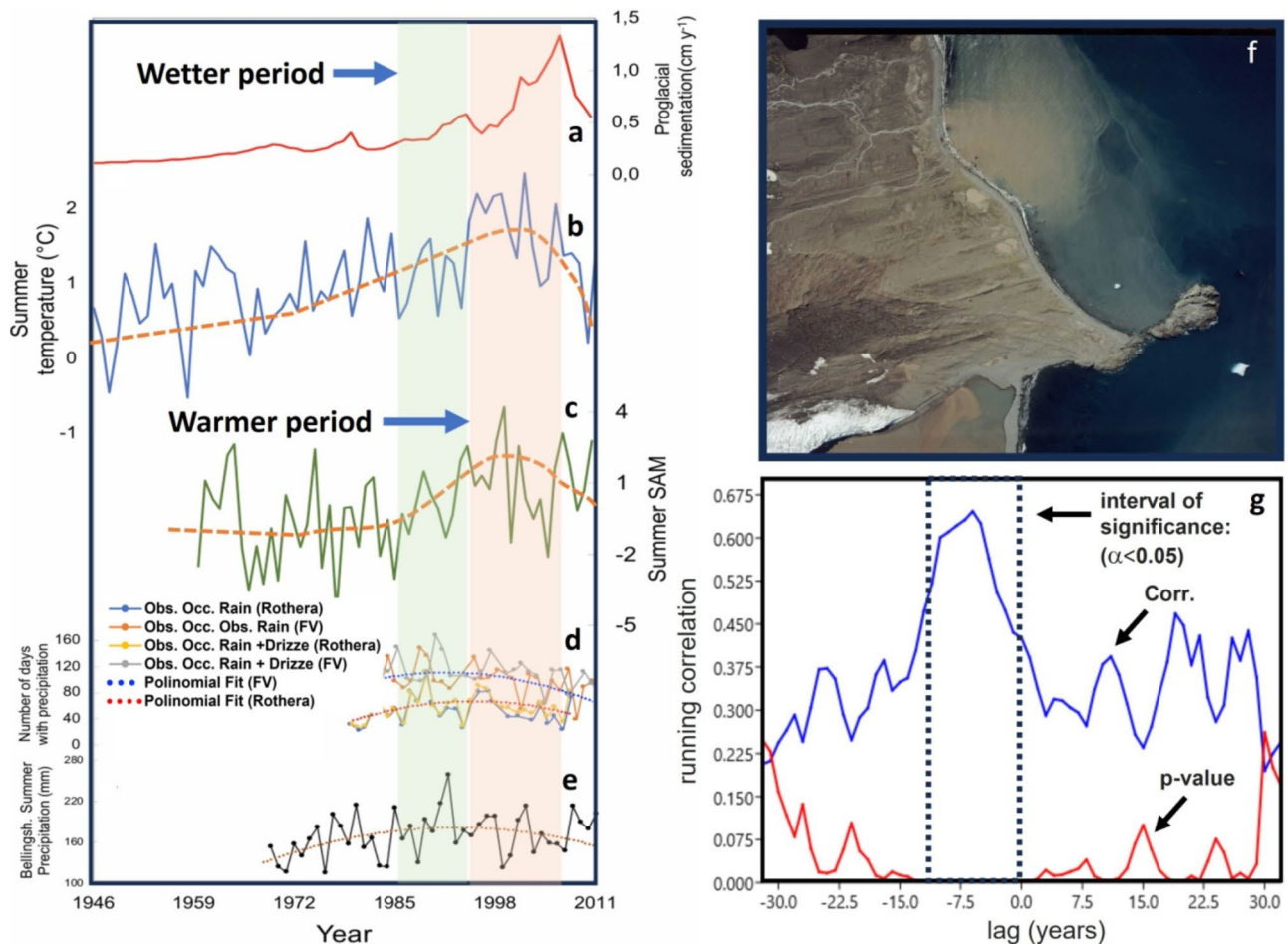


**Fig. 5.** Liquid precipitation (rain), air temperature and sedimentation rate at North Antarctic Peninsula. (a) Mean proglacial sedimentation at KGI; (b) regional summer air temperature, DJF, composite of data from Bellingshausen-March-Condandante Ferraz-Deception stations; (c) Summer SAM (Marshall et al., 2006); (d) annual number of days with rain and drizzle data from Rothera and Faraday-Vernadsky Stations (Vignon et al., 2021)<sup>42</sup>; (e) Bellingshausen Station summer precipitation (this issue); (f) sediment plume formation at proglacial site at Admiralty Bay/KGI; (g) lag-correlation between air summer temperature and sedimentation. The blue curve depicts the correlation curve with indication of the time interval in a significance level at 0.05. Dotted and dashed curves are polinomial fits at boxes (d) and (e).

that the LIA was not a seesaw-type climate event. LIA was a period of unusually short time and wide-spread cooling that lasted from about 1250 to 1860 AD<sup>47</sup> when glaciers across the North Hemisphere were significantly larger with mean annual air temperatures 1 °C lower than today.

In the NAP the hiatus in sedimentation is maintained until nearly mid-19th century and rapidly increases towards the 20th century until the great peak of the beginning of 21st century, as depicted in Fig. 2. At the Northeastern Antarctic Peninsula sector, glaciers advance also corroborate our findings where repeatedly expansions occurred around 2.4 and 1.0 kyr BP and over the last few centuries<sup>48</sup>. The sequence of sedimentation hiatuses depicted in Fig. 6 suggests that the Late Holocene Neoglacial phase in NAP/WAIS can be divided into 2 periods at the terrestrial periglacial environment: the first being characterized by an initial cooling phase, between 1.4 and 1.0 kyr BP, (corresponding to the Medieval Warm Period/Medieval Climate Anomaly- MWP) and a second by a deep cooling phase, between 800 and 200 year BP (corresponding to the North Hemisphere Little Ice Age - LIA). The MWP is a warm climate period revealed by archaeological evidence, botanic and paleoclimatic records coming from parts of the North Atlantic and North America.

At Maxwell Bay, a site in the vicinity of Fildes Peninsula (Fig. 1), where 8 of the periglacial lakes were investigated, grain size data from a Holocene sediment core<sup>17</sup> allowed distinguish a relatively warm phase dated from the MWP (when fine grains are predominated in the sediment record) from a preceding cooling phase, dated from the LIA. Maxwell Bay receives melting water from several drainage systems of KGI glaciers. Therefore, fine sediments at Maxwell Bay may reflect erosive processes at Fildes Peninsula and other adjacent ice-free areas. From this observation, and differently from the record of isolated periglacial lakes, during the on set of the cooling phase at NAP, glaciomarine shore sites still received some sediments indicating a high sensitivity to summer air temperatures.



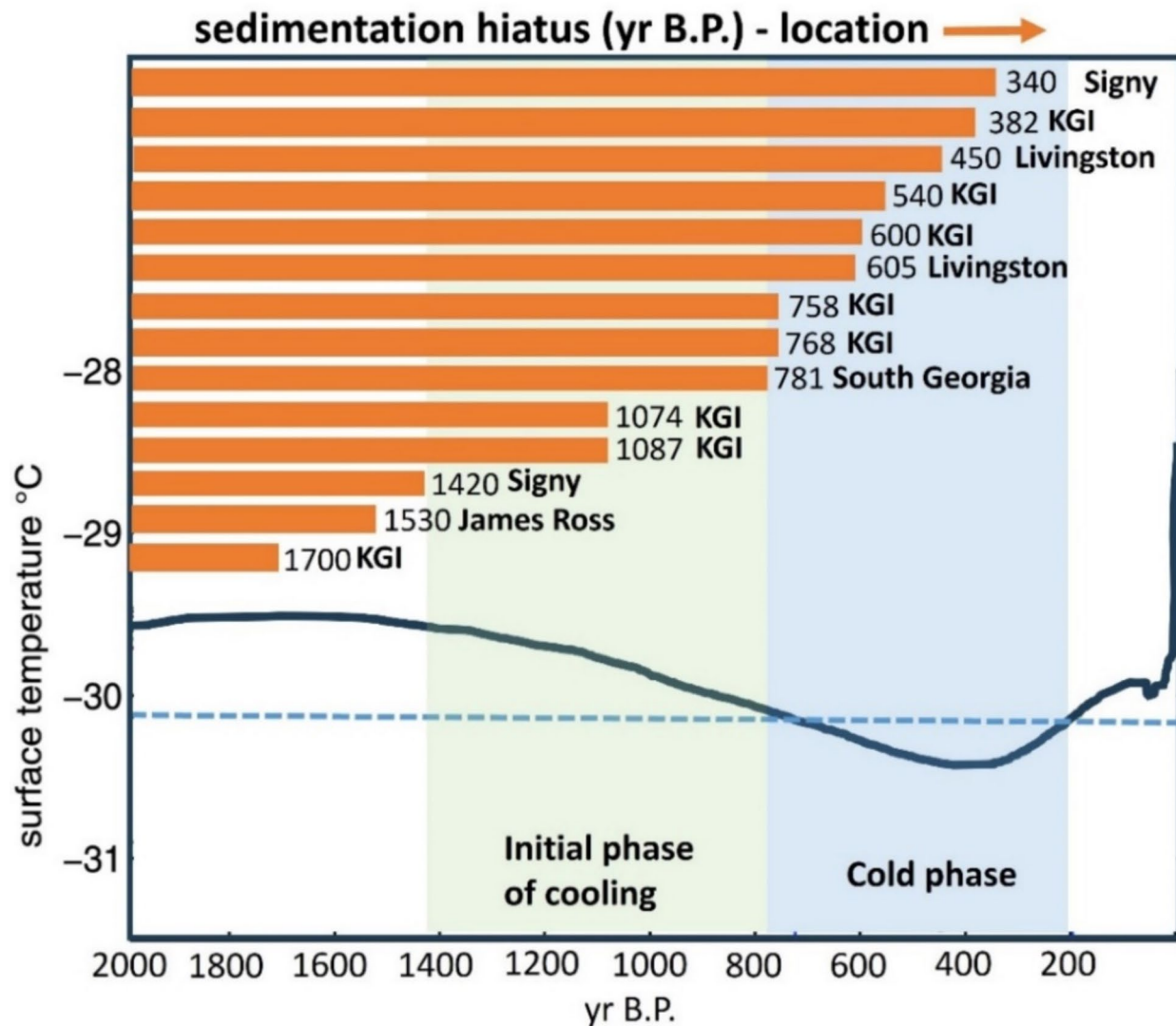


**Fig. 6.** Sediment core-top ages. Grouping of core-top ages in sediment profiles of periglacial lakes used to identify sedimentation hiatus (horizontal bars), corresponding to Table 1, from North Antarctic Peninsula and the surrounding region. The black thick line represents the mean borehole temperature obtained in WAIS Divide at the center of West Antarctica (Orsi et al., 2012); the dashed line identifies the colder phase in the last 2 kyr.

Previous studies have documented the climatic phases of the NAP and the surrounding region in the Holocene, using multiproxy approaches<sup>27</sup>. However, our understanding of the effective role of main climate drivers remain highly uncertain. In Fig. 7 we compared glacial record, an ocean record and lacustrine sedimentation histories, together with climate forcings (TSI, ENSO, CO<sub>2</sub> concentrations, summer insolation, and volcanic episodes) to investigate how these variables covariate. Volcanism used here refers to Simple Dome A (SDM-A ice core record)<sup>53</sup> (Fig. 7h) located in West Antarctica. From Fig. 7 we identified two distinct climatic phases at NAP and the surrounding region during the Late Holocene: (1) a warm phase covering the period approx. 2.0 kyr BP – 5.5 kyr BP imprinted in the three compartments ocean-cryosphere-lithosphere (lacustrine environment). This period accompanied lower ENSO activity, lower volcanism, lower summer insolation (Fig. 7j) and increased CO<sub>2</sub> (Fig. 7). Despite this condition, during the warm phase, KGI periglacial environment experienced regular swings of temperature and primary productivity as evidenced by laminated structures at Long Lake sediment core, as shown in Fig. 3; (2) an important drop in the regional average air temperature from approx. 1.7–2.0 kyr BP to nearly mid-20th century characterizing a Neoglacial phase in the regional paleoclimate history. This was evidenced by the deuterium analysis at JRI ice core<sup>49</sup> (Fig. 7f), the increase of sea ice-related diatoms (e.g.: *A. actinochilus* and *F. cylindrus*), a decrease of open water taxa (e.g.: *R. styliformis*) and decrease of total organic carbon (TOC) (Fig. 7e) from a sediment core retrieved at South Scotia Sea<sup>50</sup>. Along the Antarctic coast, the discharge of highly  $\delta^{18}\text{O}$ -depleted glacial ice (from both melting water and/or solid ice) is the sole process that can significantly reduce  $\delta^{18}\text{O}$  in seawater. Consequently,  $\delta^{18}\text{O}$  in diatoms may reflect that process. A record

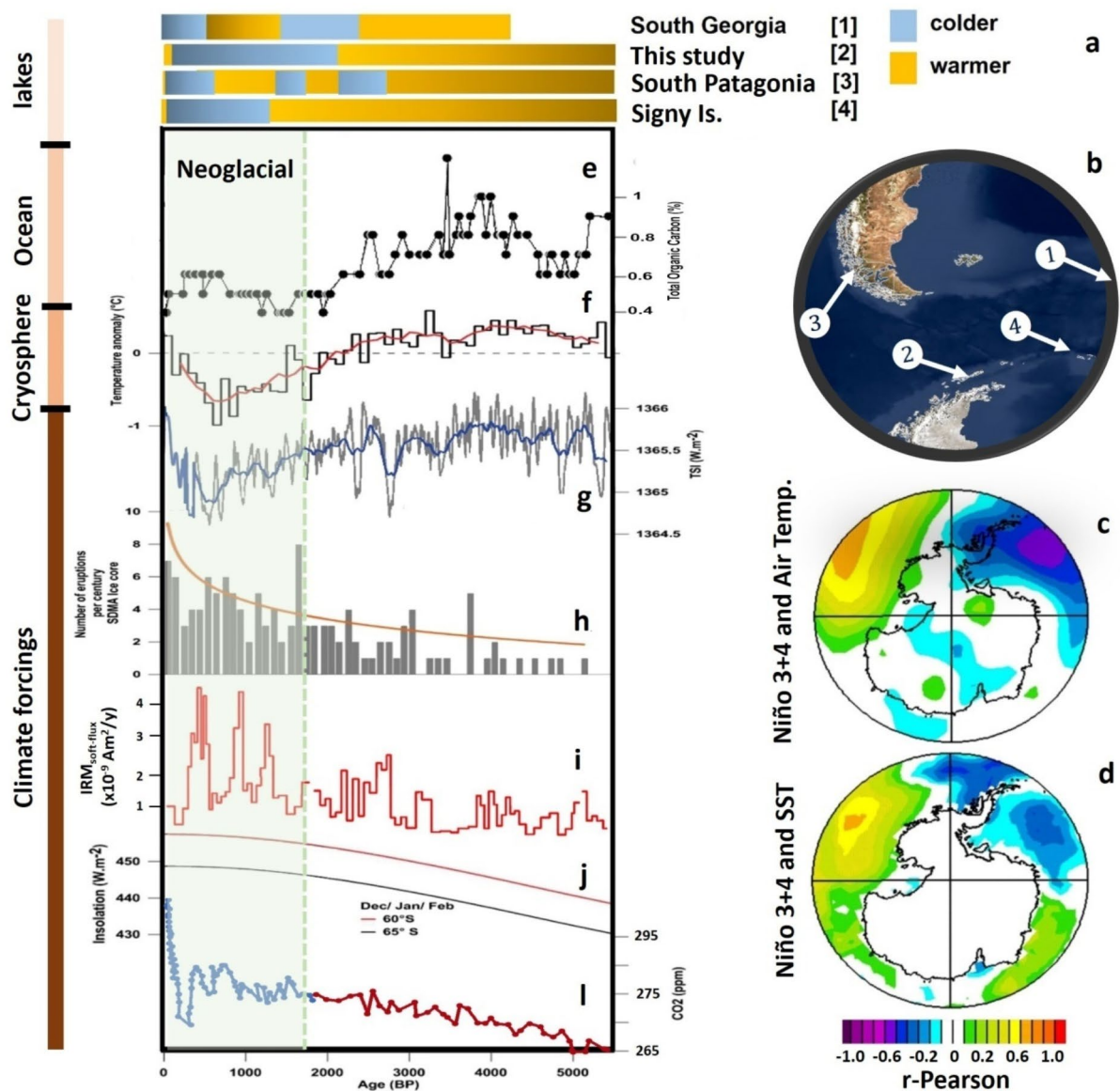


**Fig. 7.** Natural archives and parameters related to climate at North Antarctica Peninsula. (a) Summary of paleoclimate records related to Late Holocene Neoglacial: Strother et al., 2014<sup>31</sup>, 2. This issue, 3. Glasser et al., 2004<sup>64</sup>, 4. Jones et al., 2000<sup>30</sup>; (b) locations of records of "a"; (c) correlation map for surface mean annual air temperature and Niño 3 + 4 (this issue); (d) correlation map for Sea Surface Temperature and Niño 3 + 4 (this issue); (e) TOC-Total Organic Carbon (Bak et al., 2007)<sup>50</sup>; (f) air temperature reconstructed from JRI ice core (Mulvaney et al., 2012)<sup>49</sup>; (g) TSI reconstructed (Vieira et al., 2011); (h) volcanic events recorded at Simple Dome A ice core (81°39.530 S, 148°48.720 W; 621 m) and trend curve (Kurbatov et al., 2006); (i) Niño 3 + 4 reconstructed from speleothems (Zhu et al., 2017); (j) austral summer insolation at NAP; (l) Composite Antarctic Holocene CO<sub>2</sub> (Law Dome - blue curve and Dome C - red curve) Antarctic Holocene CO<sub>2</sub> (Monnin et al. 2004; MacFarling Meure et al. 2006).

from an ODP sediment core at site 1098 reported from the Western Antarctic Peninsula showed a steady decrease in the isotopic signal since the last approx. 4.0 kyr BP with a steeper trend after 2.0 kyr BP<sup>12</sup>. This behavior accompanied the periglacial sedimentation hiatus throughout the investigated region (Fig. 7a, b). When comparing the natural climate archives with parameters in Fig. 7 we identified a concomitant increase in volcanic events and decrease of total solar irradiance (TSI) during the Late Holocene Neoglacial phase. Such a combination of volcanism and TSI resulting in cooling was previously documented for the North Hemisphere during the LIA epoch when solar minima Wolf, Spörer, Maunder, and Dalton were nearly coincident with volcanic eruption sequences<sup>51</sup>, although alternative theories have also been proposed for LIA<sup>52</sup>. LIA in the North Hemisphere started around 1,300 CE<sup>53</sup> lasting around 550 years. Our database for the NAP and the surrounding region suggests that a possible volcanic trigger of the cooling is better explained by the volcanic record of

WAIS/SDM-A ice core, which depicts a steady increase in activity throughout the Late Holocene. Nonetheless, this volcanism sequence is mostly of moderate VEI (Volcanic Explosive Index) and derived from two main sources: the Southern Andes volcanic sector and from the Antarctic continent, corresponding to a regional origin. Moderate but recurring volcanism, to a lesser extent, may also act as climate forcing since the aerosol loading may reach the lower stratosphere, as experimentally demonstrated in previous studies<sup>54</sup>. Moreover, it has been claimed that decadal-paced eruptions could generate more cooling than single large eruptions if the recurrence interval is shorter than the upper ocean temperature relaxation time of decades<sup>55</sup>. Another point is the proximity of these volcanic sites to the NAP that could induce a direct impact. The SDM-A location is of relatively lower elevation, 974 m a.s.l., compared to other sites on the Antarctic Plateau but very representative of the atmospheric transport and circulation pattern enclosing the continental regions closer to the Southern Ocean and the WAIS. The constant action of cyclonic systems around 60°S favors northerly air mass incursions to West Antarctica and the advection of air parcels and terrigenous aerosols from meridional South America<sup>56</sup>. Concomitant with the increased volcanism since the last 2,000 years we observed a progressive decrease of the TSI (Fig. 7c). In Fig. 7 we show that the synchronism in total solar irradiance and volcanism is consistent with the timing when air temperature decreases and sedimentation ceases at NAP and the surrounding region. The fact that during the LIA at the NAP and the surrounding region a cooling condition was in progress, reinforces the concept of a global effect of this climatic episode. However, an issue that remains relatively unclear is the feedback amplifications involved since air temperature estimated in several places of the North Hemisphere cannot be solely explained by a lowering in solar irradiance and an increased volcanism<sup>46</sup>. In addition to solar and volcanic climatic forcings, an intensified Niño 3 + 4 index accompanied these trends (Fig. 7i). The impact of El Niño events over West Antarctica has been widely discussed<sup>57</sup>. However, such impacts are not spatially uniform. For the Amundsen and Bellingshausen Sea sectors that border the Antarctic Peninsula, intense El Niño events may lead to ice mass gain near shelves and marginal coastal zones<sup>57</sup>. Our correlation maps of Niño 3 + 4 and air temperature (Fig. 7c) and Niño 3 + 4 and SST (sea surface temperature) (Fig. 7d), using the NCEP-NCAR reanalysis II, suggest that more ENSO events can strengthen the cooling at the NAP and surrounding region (Fig. 7c, d). Therefore, in addition to the decrease in TSI and increase in volcanism, ENSO events could also play a role in the NAP Neoglacial phase despite the influence of the slight increase in CO<sub>2</sub> (on the order of 10 ppm, Fig. 7g) and the increase in austral summer insolation (maximum of 20 W m<sup>-2</sup>, Fig. 7f). The climate mechanism behind the recovery to a warming phase at the NAP and the surrounding region since mid-20th century is an issue not yet fully explained. Important controls postulated for this process are (a) more warm advection from the Subtropical Pacific Ocean, (b) an increased influence of the westerly winds from a combined positive phase of the SAM and an amplification due to the Antarctic ozone depletion<sup>58,59</sup> and (c) a higher frequency of northerly warm air mass advection, as revealed by the increasing amount of mineral dust particles reaching the NAP<sup>60</sup> and WAIS<sup>56</sup>. All these mechanisms resulting from the southward shift of the westerlies. Considering SAM reconstructions, modern values of SAM fall outside the 2σ range and such increase can only be explained if an anthropogenic component is placed as an additional driver<sup>61</sup>. The rapid air temperature increases since the late 20th century documented at the NAP and the surrounding region are also observed in southern Patagonia, reconstructed from intra-annual bands in the wood of *Nothofagus pumilio*<sup>62</sup>.

The Late Holocene Neoglacial phase extended further north from the NAP to sub-Antarctic and temperate sites as in South Georgia at 54°S<sup>63</sup> and in South and North Patagonian Ice field at 48°S and 47°S<sup>64</sup>. In South Georgia, GDGT-derived temperatures for the last 2,000 year exhibited a prevalent cold phase without an obvious MWP, which was represented only as a short-term event in comparison to its Northern Hemisphere signal recorded in the GISP2 ice core<sup>65</sup>. In Patagonia, a prolonged cold phase has been recognized from glacier advances at 2.7–2.0 kyr BP; 2.3 kyr BP; 1.6–1.4 kyr BP, and during the Little Ice Age<sup>64</sup>. The sedimentation response to cooling and the climatic characteristics presented in Fig. 7, representing the Neoglacial phase at NAP and the surrounding region, is corroborated by the negative trend in reconstructed air temperatures at 2 m over the past two millennia acquired from tree climate model simulations (CMIP6, ECHAM, and NB2014)(Supplementary information 7).

## Conclusions

From a new multi-proxy approach combining proglacial/periglacial lake sedimentation, ice core and marine records, we give new insights on the climate changes and their sedimentary implications at NAP (and the surrounding region) from Late Holocene to the contemporary era. Our results and regional data compilation recognized a scenario of high climate variability with transitions from a relatively warm climate during the onset of the Late Holocene to a Neoglacial phase comprising the 2 kyr BP until nearly the beginning of the 20th century. This cold phase extended throughout the LIA and MWP, differently from the Northern Hemisphere when these two phases were well identified separately. Although the mechanism explaining these climate swings is not yet fully described, we found concomitant changes with the decrease of total solar irradiance, increase of the moderate Andean volcanism and ENSO variability. For the contemporary age, we found that present warming period is the major controlling factor of the regional lacustrine sedimentation and that elemental Ti/Ca and Ti/Al ratios are reliable geochemical proxies of such process. Finally, considering the high number of still unexplored proglacial/periglacial lakes at NAP, our work reinforces the importance to improve the regional lacustrine paleoclimate surveys as a tool to clarify the relationship between climate changes and the evolution of the terrestrial environment in Maritime Antarctica.



## Methods

### Sediment coring and sample preparation

Sediment coring of periglacial lakes investigated in this work (Long lake, Slamnoe lake, Trigorskoe lake and Geographensee lake) at KGI started during the austral summer of 2015 in the context of the UN/FAO/IAEA project “Assessing the Impact of Climate Change and its Effects on Soil and Water Resources in Polar and Mountainous Regions, INT/5/153”, with the support of the Russian Antarctic Program and the Brazilian Antarctic Program. Sediment cores were retrieved using two types of corer, one a hammer-gravity version of a UWITEC corer equipped with a 1.2 m plastic tube installed on a fixed tripod over a floating platform and a second a Russian Sediment/Peat Borer used from the frozen surface of the lakes. Cores from proglacial shallow lakes were sampled manually with PVC tubes to minimize disturbances. Sediment cores were stored at 4 °C until analysis and transported to Brazil where non-destructive analyses were first conducted (lithological description, X-ray, and magnetic susceptibility). After that the cores were longitudinally sectioned at 1 cm resolution, under clean room conditions, and each subsample was weighed, dried at 50 °C for 24 h, powdered, and sealed in plastic 47 mm-petri dishes for radiometric dating.

### Radiometric dating and $^{210}\text{Pb}$ core chronology

Radiometric dating using  $^{210}\text{Pb}_{\text{excess}}$  was conducted using a hyper pure germanium (GeHP) detector of coaxial geometry with a diameter of 56 mm and a length of 38.5 mm. The gamma system (detector and electronics) was installed in the Laboratory of Radioecology and Global Change (LARAMG / Rio de Janeiro State University). The relative efficiency is 20%, with a resolution of 1.8 keV at 1.33 MeV and 0.850 keV at 122 keV. A very low background lead shield of 12 cm with an internal copper lining on all walls was used. Detector efficiency curves were constructed from a NIST cocktail of radionuclides composed of  $^{133}\text{Ba}$ <sup>57</sup>, Co,  $^{139}\text{Ce}$ ,  $^{85}\text{Sr}$ ,  $^{137}\text{Cs}$ <sup>54</sup>, Mn,  $^{88}\text{Y}$  and  $^{65}\text{Zn}$  in a solution of 0.5 M HCl. In addition to the natural radionuclides, we searched for  $^{137}\text{Cs}$  trace activities in all samples.

Chronologies of shallow lakes sediment cores were established using the Constant Rate of Supply (CRS)<sup>66</sup> model at 1 cm core depth resolution. Dating was corrected by the  $^{137}\text{Cs}$  peak when detected, that is attributed to the North Hemisphere 1961/62 atomic bomb test of global impact<sup>67</sup>. For the Antarctic margin, the nuclear peak corresponds to the year 1965, according to Clarke et al., 2012<sup>68</sup>. For the CRS method, we used activity data for  $^{210}\text{Pb}_{\text{excess}}$ <sup>66</sup> measured by a high-resolution GeHP gamma spectroscopy. The basic concept of the model is provided by the relationship  $^{210}\text{Pb}_{\text{excess}} = ^{210}\text{Pb}_{\text{Total}} - ^{210}\text{Pb}_{\text{Supported}}$ . Successive layers of newly deposited sediments are enriched with  $^{210}\text{Pb}_{\text{excess}}$ , which exponentially decays in the lake sediment profile. Therefore, the accumulation rate of the sediments being deposited can be estimated by a simple decay Eq. 6<sup>9</sup> as:  $\text{Activity}_{\text{Pb-210}}(t) = \text{Activity}_{\text{Pb-210}}(t=0) \cdot e^{-(\lambda_{\text{Pb-210}})t}$ , where  $\lambda_{\text{Pb-210}}$  is the radioactive decay constant of  $^{210}\text{Pb}$  equal to  $0.03114 \text{ year}^{-1}$ . Sediment layer ages are obtained by the equation as follows:

$$t_{\text{sed}} = \frac{-1}{\lambda_{210\text{pb}}} \cdot \left( 1 - \frac{\sum A_m}{\sum A_{\infty}} \right)$$

where  $\sum A_m$  represents the integrated  $^{210}\text{Pb}$  activity from the surface to depth (m) and  $\sum A_{\infty}$  is the total integrated concentration of unsupported  $^{210}\text{Pb}$ . All activities of  $^{210}\text{Pb}$  and  $^{226}\text{Ra}$  used for the CRS model were determined by high-resolution gamma spectrometry. In natural environments, factors influencing undisturbed downcore exponential decay profiles include bioturbation, diffusion, or slumping<sup>70</sup>. The average annual sedimentation rate, considering all shallow lakes investigated in this work, was obtained after establishing the chronology of each deposition layer at each sediment core separately. Then, for each period of time all the corresponding sedimentation rates were averaged by arithmetic mean, obtaining the standard deviation.

The Long Lake sediment core (code: LL2-IAEA) chronology is based on  $^{14}\text{C}$  analysis performed at Beta Analytic Laboratory AMS. Bulk sediments were acid-alkali-acid treated following standard protocols and results are reported in conventional  $^{14}\text{C}$  ages according to Stuiver & Polach (1977). Conventional  $^{14}\text{C}$  ages were calibrated using the SHCal20 calibration curve (Hogg et al., 2020). AMS results are presented in Table 3 of Supplementary information 4. AMS analysis of top sediment cores of Slamnoe lake, Trigorskoe lake and Geographensee lake were conducted at the International Chemical Analysis-US, Inc. (ICA).

### Elemental carbon and nitrogen and isotope measurements

Samples were dried at 40 °C, and inorganic carbon was removed prior to analysis of %C and  $^{13}\text{C}/^{12}\text{C}$  by acid fumigation method<sup>71</sup>. Moistened subsamples were exposed to the exhalation of HCl in a desiccator overnight; afterwards, the samples were dried at 40 °C before measurement. The N(%) and  $^{15}\text{N}/^{14}\text{N}$  analyses were performed with unacidified samples. The stable N and C isotope ratios and the C and N concentrations were measured using an elemental analyser (Vario Isotope Select, Elementar, Langenselbold, Germany) coupled to an isotope ratio mass spectrometer (Isoprime 100, Elementar, Langenselbold, Germany) located at the Soil and Water Management and Crop Nutrition Laboratory of the Joint FAO/IAEA Centre of Nuclear Techniques in Food and Agriculture. The N isotope ratios were calibrated against the reference materials IAEA-N-1 and IAEA-N-2. Calibration of C isotope ratios was performed using two laboratory standards, a sugar beet standard with  $\delta^{13}\text{C}$  -26.07‰ and a sugar cane standard with  $\delta^{13}\text{C}$  -10.95‰. Both laboratory standards were calibrated against IAEA-CH-6 and IAEA-CH-7. The C and N concentrations were calibrated against the reference material NIST 1547. The analytical accuracies of the measured standards and reference materials were  $\delta^{15}\text{N}$  -0.05‰ and  $\delta^{13}\text{C}$

-0.03‰, and the analytical precisions were  $\pm 0.19\text{‰}$  for  $^{15}\text{N}$  and  $\pm 0.12\text{‰}$  for  $^{13}\text{C}$  isotopes. Stable isotope data were reported as delta values (‰) relative to air for  $^{15}\text{N}$  and VDPB for  $\delta^{13}\text{C}$ .

### XRF scanning

XRF Core Scanner data were collected every 2 mm downcore using generator settings of 20, 30 and 50 kV, a sampling time of 10 s directly on the split core surface of the archive half with XRF Core Scanner III (AVAATECH Serial No. 12) at MARUM, University of Bremen. The split core surface was covered with a 4-micron thin SPEXCerti Prep Ultralene1 foil to avoid contamination of the XRF measurement unit and desiccation of the sediment. The reported data were acquired by an SGX Sentsortech Silicon Drift Detector (Model SiriusSD<sup>7</sup> D65133Be-INF with 133 eV X-ray resolution), a Topaz-X High-Resolution Digital MCA, and an Oxford Instruments 100 W Neptune X-ray tube with rhodium (Rh) target material. Raw data spectra were processed by the analysis of X-ray spectra by the iterative least square software (WIN AXIL) package from Canberra Eurisys. We selected Zr, Rb, Al, Si, K, Ca, Ti, Al, Fe and Mn as elements, from which we calculated several ratios as proxies for paleoenvironmental change. High-resolution XRF scanning techniques are useful for inferring interannual paleolimnological changes in Subantarctic proglacial lakes during the processes of centennial glacier retreat<sup>23</sup>. XRF is especially appropriate for inferring events and increased catchment erosion inputs (i.e., Ti/Ca and Ti/Al<sup>72–74</sup>).

### Data availability

The authors declare that fundamental databases with support the findings of this study are available within the paper and its supplementary information files. Complementary geochemical data used here are available from the corresponding author on reasonable request.

Received: 3 January 2024; Accepted: 17 December 2024

Published online: 30 December 2024

### References

1. Bromwich, D. H. et al. Central West Antarctica among the most rapidly warming regions on Earth. *Nat. Geosci.* **6**, 139–145 (2013).
2. Watcham, E. P. et al. A new Holocene relative sea level curve for the South Shetland Islands, Antarctica. *Quat. Sci. Rev.* **30**, 3152–3170 (2011).
3. Lüning, S., Galka, M. & Vahrenholt, F. The medieval climate anomaly in Antarctica. *Palaeogeogr. Palaeoclimatol. Palaeoecol.* **532**, 1–18 (2019).
4. Abram, N. J. et al. Acceleration of snow melt in an Antarctic Peninsula ice core during the twentieth century. *Nat. Geosci.* **6**, 404–411 (2013).
5. Feldmann, J. & Levermann, A. Collapse of the West Antarctic Ice Sheet after local destabilization of the Amundsen Basin. *Proc. Natl. Acad. Sci. U.S.A.* **112**, 14191–14196 (2015).
6. Turner, J. et al. Absence of 21st century warming on Antarctic Peninsula consistent with natural variability. *Nature* **535**, 411–415 (2016).
7. Kim, J. et al. New particle formation events observed at King Sejong Station, Antarctic Peninsula – Part 1: Physical characteristics and contribution to cloud condensation nuclei. *Atmos. Chem. Phys.* **19**, 7583–7594 (2019).
8. Ding, Q. & Steig, E. J. Temperature change on the Antarctic Peninsula linked to the tropical Pacific. *J. Clim.* **26**, 7570–7585 (2013).
9. Rahaman, W., Chatterjee, S., Ejaz, T. & Thamban, M. Increased influence of ENSO on Antarctic temperature since the Industrial Era. *Sci. Rep.* **9**, 1–12 (2019).
10. Turner, J., Lachlan-Cope, T. A., Colwell, S., Marshall, G. J. & Connolley, W. M. Significant warming of the antarctic winter Troposphere. *Sci. (80-)* **311**, 1914–1917 (2006).
11. Russell, A. & McGregor, G. R. Southern hemisphere atmospheric circulation: Impacts on Antarctic climate and reconstructions from Antarctic ice core data. *Clim. Change* **99**, 155–192 (2010).
12. Pike, J., Swann, G. E. A., Leng, M. J. & Snelling, A. M. Glacial discharge along the West Antarctic Peninsula during the Holocene. *Nat. Geosci.* **6**, 199–202 (2013).
13. Wille, J. D. et al. Intense atmospheric rivers can weaken ice shelf stability at the Antarctic Peninsula. *Commun. Earth Environ.* **3**, 1–15 (2022).
14. Assmann, K. M., Darelus, E., Wählin, A. K., Kim, T. W. & Lee, S. H. Warm Circumpolar Deep Water at the western Getz Ice Shelf Front, Antarctica. *Geophys. Res. Lett.* **46**, 870–878 (2019).
15. Simões, J. C. et al. Ice core study from the King George Island, South Shetlands, Antarctica. *Pesqui. Antártica Bras.* **4**, 9–23 (2004).
16. Fernandoy, F., Meyer, H. & Tonelli, M. Stable water isotopes of precipitation and firn cores from the northern Antarctic Peninsula region as a proxy for climate reconstruction. *Cryosph.* **6**, 313–330 (2012).
17. Hass, H. C., Kuhn, G., Monien, P., Forwick, M. & Sea, W. Climate fluctuations during the past two millennia as recorded in sediments from Maxwell Bay, South Shetland Islands, in *Fjord Systems and Archives* (ed. Howe, J. A., Austin, W. E. N., Forwick, M. & Paetzel, M.) vol. 344 243–260 (The Geological Society of London, 2010).
18. Penck, A. & Brückner, E. *Die Alpen im Eiszeitalter*. (Leipzig, C. and Tauchnitz, H., (1909).
19. Fossum, K. N. et al. Summertime primary and secondary contributions to southern ocean cloud condensation nuclei. *Sci. Rep.* **8**, 1–15 (2018).
20. Petsch, C. et al. An inventory of glacial lakes in the South Shetland Islands (Antarctica): Temporal variation and environmental patterns. *Acad. Bras. Cienc.* **94**, 1–26 (2022).
21. Mavlyudov, B. R. Equilibrium line altitude on Bellingshausen Ice Dome, Antarctic. *Ice Snow* **4**, 72–84 (2023).
22. Braithwaite, R. J. & Raper, S. C. B. Glaciological conditions in seven contrasting regions estimated with the degree-day model. *Ann. Glaciol.* **4**, 297–302 (2007).
23. García-Rodríguez, F. et al. Centennial glacier retreat increases sedimentation and eutrophication in Subantarctic periglacial lakes: a study case of Lake Uruguay. *Sci. Total Environ.* **754**, 1–35 (2021).
24. Mesa-Fernández, J. M. et al. Paleocirculation and paleoclimate conditions in the western Mediterranean basins over the last deglaciation: new insights from sediment composition variations. *Glob. Planet. Change* **209**, 103732 (2022).
25. Wrona, R. Cambrian limestone erratics in the tertiary glacio-marine sediments of King George Island, West Antarctica. *Pol. Polar Res.* **10**, 533–553 (1989).
26. Björck, S. et al. Late Holocene palaeoclimatic records from lake sediments on James Ross Island, Antarctica. *Palaeogeogr. Palaeoclimatol. Palaeoecol.* **121**, 195–220 (1996).

27. Barión, P. A. H. et al. The impact of Holocene deglaciation and glacial dynamics on the landscapes and geomorphology of Potter Peninsula, King George Island (Isla 25 Mayo), NW Antarctic Peninsula. *Front. Earth Sci.* 1–38. <https://doi.org/10.3389/feart.2022.1073075> (2023).
28. Björck, S., Håkansson, H., Zale, R., Karlen, W. & Jonsson, B. L. A late Holocene lake sediment sequence from Livingston Island, South Shetland Islands, with palaeoclimatic implications. *Antarct. Sci.* 3, 61–72 (1991).
29. Björck, S., Håkansson, H., Olsson, S. & Lena, B. Palaeoclimatic studies in South Shetland Islands, Antarctica, based on numerous stratigraphic variables in lake sediments. *J. Paleolimnol.* 8, 233–272 (1993).
30. Jones, V. J. et al. Palaeolimnological evidence for marked Holocene environmental changes on Signy Island, Antarctica. *Holocene* 10, 43–60 (2000).
31. Strother, S. et al. Changes in Holocene climate and the intensity of Southern Hemisphere Westerly Winds based on a high-resolution palynological record from sub-antarctic South Georgia. *Holocene* 25, 263–279 (2015).
32. Piccini, C. et al. Prokaryotic richness and diversity increased during Holocene glacier retreat and onset of an Antarctic Lake. *Nat. Commun. Earth Environ.* 5, 1–11 (2024).
33. Haltia-Hovi, E., Saarinen, T. & Kukkonen, M. A 2000-year record of solar forcing on varved lake sediment in eastern Finland. *Quat. Sci. Rev.* 26, 678–689 (2007).
34. Taylor, J. C., Cocquyt, C., Karthick, B. & Van de Vijver, B. Analysis of the type of *Achnanthes exigua* Grunow (Bacillariophyta) with the description of a new Antarctic diatom species. *Fottea* 14, 43–51 (2014).
35. Fretwell, P. T., Hodgson, D. A., Watcham, E. P., Bentley, M. J. & Roberts, S. J. Holocene isostatic uplift of the South Shetland Islands, Antarctic Peninsula, modelled from raised beaches. *Quat. Sci. Rev.* 29, 1880–1893 (2010).
36. Tierney, J. E. & Tingley, M. P. A TEX 86 surface sediment database and extended bayesian calibration. *Sci. Data.* 2, 1–10 (2015).
37. Shen, J. et al. Ti content in Huguangyan maar lake sediment as a proxy for monsoon-induced vegetation density in the Holocene. *Geophys. Res. Lett.* 40, 5757–5763 (2013).
38. Orr, A. et al. Characteristics of summer airflow over the Antarctic Peninsula in response to recent strengthening of Westerly circumpolar winds. *J. Atmos. Sci.* 65, 1396–1413 (2008).
39. Zou, X. et al. Strong warming over the Antarctic Peninsula during Combined Atmospheric River and Foehn events: contribution of Shortwave Radiation and Turbulence. *J. Geophys. Res. Atmos.* 128, 1–23 (2023).
40. Marshall, G. J., Orr, A., van Lipzig, N. P. M. & King, J. C. The impact of a changing Southern Hemisphere Annular Mode on Antarctic Peninsula summer temperatures. *J. Clim.* 19, 5388–5404 (2006).
41. Pollard, D., Deconto, R. M. & Alley, R. B. Potential Antarctic ice sheet retreat driven by hydrofracturing and ice cliff failure. *Earth Planet. Sci. Lett.* 412, 112–121 (2015).
42. Vignon, E., Roussel, M. L., Gorodetskaya, I. V., Genthon, C. & Berne, A. Present and Future of Rainfall in Antarctica Geophysical Research letters. *Geophys. Res. Lett.* 48, 1–13 (2021).
43. MARSHALL, G. J., ORR, A., VAN LIPZIG, N. P. M. & KING, J. C. The impact of a changing Southern Hemisphere Annular Mode on Antarctic. *J. Clim.* 19, 5388–5404 (2006).
44. Bintanja, R. The local Surface Energy Balance of the Ecology Glacier, King George Island, Antarctica: Measurements and modelling. *Antarct. Sci.* 7, 315–325 (1995).
45. Zhang, T. et al. Warming-driven erosion and sediment transport in cold regions. *Nat. Rev. Earth Environ.* 3, 832–851 (2022).
46. Orsi, A. J., Cornuelle, B. D. & Severinghaus, J. P. Little ice age cold interval in West Antarctica: Evidence from borehole temperature at the West Antarctic ice sheet (WAIS) divide. *Geophys. Res. Lett.* 39, 1–7 (2012).
47. Wanner, H., Pfister, C. & Neukom, R. The variable European little ice age the variable European little ice age. *Quat. Sci. Rev.* 287, (2022).
48. Kaplan, M. R. et al. Holocene glacier behavior around the northern Antarctic Peninsula and possible causes. *Earth Planet. Sci. Lett.* 534, 1–12 (2020).
49. Mulvaney, R. et al. Recent Antarctic Peninsula warming relative to Holocene climate and ice-shelf history. *Nature* 489, 141–144 (2012).
50. Bak, Y. S., Yoo, K. C., Yoon, H., Il, Lee, J. D. & Yun, H. Diatom evidence for Holocene paleoclimatic change in the South Scotia Sea. *Geosci. Journal.* 11, 11–22 (2007).
51. Mann, M. E. et al. Global Signatures and Dynamical origins of the little ice age and medieval climate anomaly. *Sci. (80-)*. 326, 1256–1260 (2009).
52. Miles, M. W., Andresen, C. S. & Dylmer, C. V. Evidence for extreme export of Arctic Sea ice leading the abrupt onset of the little ice age. *Sci. Adv.* 6, 1–6 (2020).
53. Miller, G. H. et al. Abrupt onset of the little ice age triggered by volcanism and sustained by sea-ice / ocean feedbacks and sustained by sea-ice / ocean feedbacks. *Geophys. Res. Lett.* 39, 1–5 (2012).
54. Berthet, G. et al. Impact of a moderate volcanic eruption on chemistry in the lower stratosphere: Balloon-borne observations and model calculations. *Atmos. Chem. Phys.* 17, 2229–2253 (2017).
55. Schneider, D. P., Ammann, C. M., Otto-bliesner, B. L. & Kaufman, D. S. Climate response to large, high-latitude and low-latitude volcanic eruptions in the community climate system model. *J. Geophys. Res.* 114, 1–21 (2009).
56. Dixon, D. A. et al. An ice-core proxy for northerly air mass incursions into West Antarctica. *Int. J. Climatol.* 32, 1455–1465 (2011).
57. Paolo, F. S. et al. Response of Pacific-sector Antarctic ice shelves to the El Niño/Southern oscillation. *Nat. Geosci.* 11, 121–126 (2018).
58. Thompson, D. W. J., Baldwin, M. P. & Solomon, S. Stratosphere – Troposphere Coupling in the Southern Hemisphere. *J. Atmos. Sci.* 62, 708–715 (2005).
59. Yang, X. Y., Huang, R. X. & Wang, D. X. Decadal changes of wind stress over the Southern Ocean associated with Antarctic ozone depletion. *J. Clim.* 20, 3395–3410 (2007).
60. McConnell, J. R., Aristarain, A. J., Banta, J. R., Edwards, P. R. & Simões, J. C. 20th-Century doubling in dust archived in an Antarctic Peninsula ice core parallels climate change and desertification in South America. *Proc. Natl. Acad. Sci. U S A.* 104, 5743–5748 (2007).
61. King, J., Anchukaitis, K. J., Allen, K., Vance, T. & Hessler, A. Trends and variability in the Southern Annular Mode over the common era. *Nat. Commun.* 14, 1–14 (2023).
62. Masiokas, M. & Villalba, R. Climatic significance of intra-annual bands in the wood of *Nothofagus pumilio* in southern Patagonia. *Trees - Struct. Funct.* 18, 696–704 (2004).
63. Foster, L. C. et al. Development of a regional glycerol dialkyl glycerol tetraether (GDGT)-temperature calibration for Antarctic and sub-antarctic lakes. *Earth Planet. Sci. Lett.* 433, 370–379 (2016).
64. Glasser, N. F., Harrison, S., Winchester, V. & Aniya, M. Late pleistocene and holocene palaeoclimate and glacier fluctuations in Patagonia. *Glob. Planet. Change.* 43, 79–101 (2004).
65. Grootes, P. M. & Stuiver, M. Oxygen 18/16 variability in Greenland snow and ice with 10 -3- to 105-year time resolution. *J. Geophys. Res.* 102, (1997). 26,455 – 26,470.
66. Appleby, P. G. & Oldfield, F. The calculation of lead-210 dates assuming a constant rate of supply of unsupported 210Pb to the sediment. *Catena* 5, 1–8 (1978).
67. UNSCEAR. Sources and Effects of Ionizing Radiation, United Nations Scientific Committee on the Effects of Atomic Radiation UNSCEAR 2000 Report to the General Assembly, with Scientific Annexes. UNSCEAR 2000 Report vol. I. (2000).



68. Clarke, L. J., Robinson, S. A., Hua, Q., Ayre, D. J. & Fink, D. Radiocarbon bomb spike reveals biological effects of antarctic climate change. *Glob Chang. Biol.* **18**, 301–310 (2012).
69. Ivanovich, M., Harmon, R. S., Russell, S. & (*Uranium-series Disequilibrium: Applications to Earth, Marine, and Environmental Sciences* (Clarendon, 1992).
70. Farmer, J. G. Determination of sedimentation rates in lake ONTARIO USING THE 210Pb dating method. *Can. J. Earth Sci.* **15**, 431–437 (1978).
71. Harris, D., Horwath, W. R. & van Kessel, C. Acid fumigation of soils to remove carbonates prior to total organic carbon or CARBON-13 isotopic analysis. *Soil. Sci. Soc. Am. J.* **65**, 1853–1856 (2001).
72. Haberzettl, T. et al. Late Pleistocene dust deposition in the Patagonian steppe - extending and refining the paleoenvironmental and tephrochronological record from Laguna Potrok Aike back to 55 ka. *Quat Sci. Rev.* **28**, 2927–2939 (2009).
73. Pérez, L., García-Rodríguez, F. & Hanebuth, T. J. J. Variability in terrigenous sediment supply offshore of the Río De La Plata (Uruguay) recording the continental climatic history over the past 1200 years. *Clim. Past.* **12**, 623–634 (2016).
74. Pérez, L. et al. Climatic oscillations modulating the late holocene fluvial discharge and terrigenous material supply from the Río De La Plata into the Southwestern Atlantic Ocean. *J. Sediment. Environ.* **3**, 205–219 (2018).

## Acknowledgements

This work was supported by the UN (United Nations)-IAEA (International Atomic Energy Agency)/FAO (Food and Agriculture Organization) Technical Cooperation Program through the INT/5/153 and INT/5/156 project “Assessing the Impact of Climate Change and its Effects on Soil and Water Resources in Polar and Mountainous Regions”. We also thank the Russian Antarctic Expedition, the Bellingshausen Russian Station and the Brazilian Antarctic Program/SECIRM (Secretaria da Comissão Interministerial para os Recursos do Mar) /PROANTAR (Programa Antártico Brasileiro) for logistic support at King George Island/Antarctica and INCT(Instituto Nacional de Ciência e Tecnologia) -Criosfera/MCTIC (Ministério de Ciência e Tecnologia e Inovação) / CNPq (Conselho Nacional de Desenvolvimento Científico e Tecnológico) and CNPq project 440899/2023-0 (Rios Atmosféricos da Antártica). We also express our thanks to Mr. Vasily Boldin for building the floating platform used for coring the Antarctic lakes. S. Verkulich acknowledges financial support from the Russian Science Foundation, project No. 22-27-00437. B. Mavlyudov was supported by the Russian state program (AAAA-A19-119022190172-5, FMGE-2019-0004). We thank Roberta Priori for editing figures.

## Author contributions

H. E. General concept of the manuscript/Paleoclimate description and text writing; S.V. General concept of the manuscript/Paleolimnological description and text writing; M.P.E. Use of frequency decomposition methods, spectral analysis and text writing; B. M. Reconstruction and long term in situ measurements of Equilibrium Line Altitude at King George Island and text writing; S.K. Lipid analysis, 14 C model and text revision; A.B.J.O. Text and graphic formatting; M.V.L. 210Pb dating and melting model; G.D. Project PI in the IAEA/FAO; C and N isotope analysis; Z.P. Diatom analysis; F.G-R. Elemental composition analysis in sediment cores by XRF and text writing; A. A. N. Magnetic susceptibility analysis and text comments; S. J. G. Jr. Sediment coring in Antarctica; R. C. A. Magnetic susceptibility analysis and text comments; M. H. C and N isotope analysis; J. S. General text revision and text comments; C. R. C and N isotope analysis; A. C. Additional gamma spectrometry for 210Pb; R. G. C and N isotope analysis; M. H S. Use of climate computational model for the study region.

## Declarations

### Competing interests

The authors declare no competing interests.

### Additional information

**Supplementary Information** The online version contains supplementary material available at <https://doi.org/10.1038/s41598-024-83754-0>.

**Correspondence** and requests for materials should be addressed to H.E.

**Reprints and permissions information** is available at [www.nature.com/reprints](http://www.nature.com/reprints).

**Publisher's note** Springer Nature remains neutral with regard to jurisdictional claims in published maps and institutional affiliations.

**Open Access** This article is licensed under a Creative Commons Attribution-NonCommercial-NoDerivatives 4.0 International License, which permits any non-commercial use, sharing, distribution and reproduction in any medium or format, as long as you give appropriate credit to the original author(s) and the source, provide a link to the Creative Commons licence, and indicate if you modified the licensed material. You do not have permission under this licence to share adapted material derived from this article or parts of it. The images or other third party material in this article are included in the article's Creative Commons licence, unless indicated otherwise in a credit line to the material. If material is not included in the article's Creative Commons licence and your intended use is not permitted by statutory regulation or exceeds the permitted use, you will need to obtain permission directly from the copyright holder. To view a copy of this licence, visit <http://creativecommons.org/licenses/by-nc-nd/4.0/>.

© The Author(s) 2024